



EXPOSURE

Alpbach Team Blue

EXoPlanet Origins and Stellar Ultraviolet Regime Explorer

Science Team: M. Aquilina, M. Cano Amoros, S. Gasparini, A. Herrijgers, V. K. Simon

Payload Team: V. D. Cardinale, C. Farret Jentink, S. Green, S. Truelsen, S. Zivithal

Engineering Team: P. Gowran, I. Pitz, T. Pospíšil, K. Serafin, G. Trindade

Tutors: G. De Marco, J. Loicq

July 20th, 2023

Abstract: Various missions, either operating or in development, are currently covering a wide range of wavelengths, from the optical regime to the mid-infrared. We propose a new mission called EXPOSURE, dedicated to studying exoplanet systems in the UV range. Particularly, EXPOSURE will measure the Lyman alpha absorption of >400 exoplanets and will resolve the Lyman alpha radial velocity profile for most of these. A major focus of the mission will be studying the variability of NUV radiation of ~200 stars hosting exoplanets. And therefore, it will also be the first mission to be able to detect a significant amount of so-called Light Echoes of Exoplanets. EXPOSURE will lead to considerably more observation time and sensitivity in the UV than what has ever been available in the past, and it is fully dedicated to exoplanets. Besides, the mission includes reserved time to look at exoplanets simultaneous with other ground based or space observatories - enabling detailed stellar activity characterization. Altogether, we believe EXPOSURE will revolutionise the field of exoplanets.

1 Introduction

The EXoPlanet Origins and Stellar Ultraviolet Regime Explorer (EXPOSURE) will embark on a mission to unravel the origins and evolution of exoplanets in the environment of their host stars in the UV regime. It will enable breakthrough science in a part of the electromagnetic spectrum that has remained largely unexplored due to small telescope sizes and low instrument throughputs. EXPOSURE's 4.2-meter aperture, combined with the fact that it has been optimised for the UV spectrum since the very first stages of its development, will bring unprecedented sensitivity in the near-, and far-UV. Based on sensitivity calculations, we estimate a sensitivity gain of a factor of 70 with respect to Hubble in Lyman-alpha spectroscopy (far-UV, 121 nm) (Gull et al. 1986). Such sensitivity will allow us to enable groundbreaking science in the following exoplanetary science fields:

- Constrain in great detail the (astro-)physical processes driving formation and evolution of exoplanets by providing a large statistical sample of planetary mass-loss.

- Explore in great depth the stellar and planetary parameters that allow for the formation of life.
- Detect new habitable zone planets around M-dwarfs by temporally resolving flares as they reflect on the planet surfaces.
- Combining our observations with observations made by ground and space based telescopes (for example JWST, Gaia, PLATO, ESPRESSO) will complement the understanding we have of the formation and characterisation of exoplanetary atmospheres.

Studying these science cases will be vital to understanding the occurrence rate of potentially habitable worlds, and with that, answering the age-old question on whether we are alone in the universe.

1.1 Atmospheric characterisation through Lyman-alpha absorption

In Figure 1 we find a mass-radius diagram of exoplanets, with a few mass-radius relations indicating a number of interior compositions. Looking at the demographics in this Figure, we can make an interesting observation: If we look at the

histogram of planet radii in Figure 1, we find the radius valley - separating the super-Earth planets (1.2-2 radii) from the sub-Neptune planets (2-3 Earth radii). It is of unknown origin, but the hypothesis is that atmospheric escape plays an important role in its formation (Owen & Lai 2018). EXPOSURE will allow the study of atmospheric escape for a large sample of exoplanets, over a large range of exoplanetary parameters by observing Lyman-alpha absorption during exoplanet transits. This will provide valuable input on atmospheric escape parameters for planetary evolution modelling (Bern Model (Mordasini et al. 2012, Affolter et al. 2023), JADE (Attia et al. 2021))

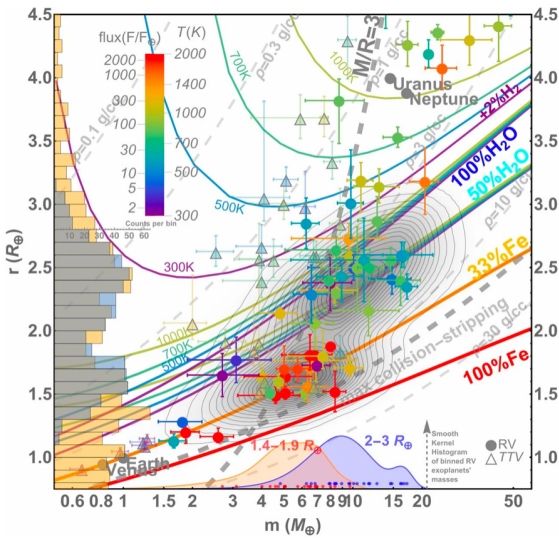


Figure 1: Mass-radius relations for various planetary compositions. The radius valley can be seen in the histogram on the vertical axis. (Zeng et al. 2019)

Some of the strongest detections of atmospheric escape have been detected using Lyman-alpha. Examples include HD209458b (Vidal-Madjar et al. 2003), and HD189733b (Lecavelier des Etangs et al. 2010). Because Lyman-alpha probes neutral hydrogen, these detections are sensitive to the very upper regions of the planet's atmosphere; their exospheres. The detection of evaporating hydrogen in close-in sub-Neptunes would show that this most frequent known type of planet has accreted primordial (nebular) atmospheres (Owen & Wu, 2013). This would give support to the view that the radius valley was indeed formed through the evaporation of primordial H/He atmospheres of rocky (silicate-iron) cores (Owen & Wu 2013, Jin & Mordasini 2018). This would have two important implications: first, it would show that these planets have formed early during the presence of the protoplanetary gas disk. Such an early formation is also suggested by modern formation models for the solar system terrestrial planets (e.g., Broz et al. 2021) and would imply the prevalence of magma-H/He reactions for young terrestrial planets. This has in turn strong consequences for the geophysical evolution of the planets and their habitability, for

example, via an intrinsic water production for Earth from the silicate-hydrogen reactions (Young et al. 2023). Second, the detection of escaping He in sub-Neptunes would rule out that these are water worlds without primordial H/He. Besides, rocky cores with H/He atmospheres, a composition with ~50% water in mass but no H/He can also explain the observed valley and the bulk densities of the known sub-Neptunes. Because of the degeneracy of the mass-radius relation, both such compositions can explain the currently available data. EXPOSURE will break this degeneracy by observing over 400 targets, well over 1 order of magnitude more than what has been observed to date. Crucially, a water poor composition would be in striking contrast with the most fundamental prediction of numerous independent modern formation models including (e.g., Venturini et al. 2021). All these models predict that Type I orbital migration (torques generated by density waves, which are triggered within the gaseous matter near a planet's Lindblad resonances (A M Mandel, 2007)) should bring protoplanets in the sub-Neptune range from beyond the iceline close to the host star. If we could reveal that in reality sub-Neptunes are rocky cores plus H/He, this would require very substantial changes in our basic picture of planet formation and call for a deep revision of disk models, migration models, or models of desiccation by short-lived radionuclides.

Our community is on the verge of detecting hundreds of planets amenable to characterisation, with missions like TESS, ESPRESSO, and PLATO. The climate and potential habitability of terrestrial planets depends on their ability to resist atmospheric erosion and subsequent loss of water (Yoshida et al. 2022, Johnstone, 2020), and to adapt to various physico-chemical processes in the upper atmosphere (e.g., the formation of a protective ozone layer through UV photodissociation of oxygen) (Mol Lous et al. 2022, Pierrehumbert et al. 2011). While these processes have been studied extensively in the solar system, close-in exoplanets in the HZ of M dwarfs – active for billions of years – evolve in more diverse and aggressive regimes of irradiation, wind, and magnetic interactions (Atri et al. 2012, do Amaral et al. 2022). Similarly, properties of gas escaping from a temperate, terrestrial planet will inform us of its nature, its atmospheric resilience, and whether it is a good candidate for habitability. Our current understanding of variability of primordial envelopes around exoplanets is limited. Which planets keep their atmosphere over time? And what roles do the orbital migration, X-UV flux, and planet bulk properties play in this? Ultimately, the atmospheric stability determines the fate of a planet's habitable properties.

1.2 Optimal UV insolation zone

In the quest for extraterrestrial life, the presence of liquid water on the surface was the main focus of search. However, in order to further constrain search for potentially habitable planets,

other thresholds within which life can emerge, such as extreme temperatures, pressures and radiation should be studied as well. As an example, extremophiles¹ offer valuable insights into these limits through research on their survival conditions. One of these is the radiophile, which is able to persist high exposures of radiation, for example in UV.

UV radiation can destroy biomolecules (Sagan et al. 1973) and cause damage to proteins and lipids of cells (Buccino et al. 2007). On the other hand, UV radiation can have prebiotic consequences. Experimental studies (Ritson & Sutherland, 2012 and others) have shown that 200-280 nm UV radiation plays an important role for the formation of ribonucleic acid (RNA), i.e. the foundational components for life (Rimmer et al. 2018). Based on these irradiance studies, Spinelli et al. (2023) defined a zone of optimal UV irradiation received by an exoplanet from its host star, which they call UV Habitability Zone (UHZ). As inner boundary, Spinelli et al. (2023) use the definition from Buccino, Lemarchand & Mauas (2007), which relies on double the UV radiation that reached the atmosphere of Earth 3.8 Gyrs ago, i.e. $2 \times 5.2 \times 10^3 \text{ erg cm}^{-2} \text{ s}^{-1}$. As the outer boundary, Spinelli et al. (2023) take the threshold found by Rimmer et al. (2018), namely $45 \text{ erg cm}^{-2} \text{ s}^{-1}$. Figure 2 shows planets in the Circumstellar Habitable Zone (CHZ) (green region) from which NUV flux data of the host star is available, as well as the UHZ (for various atmospheric transmission factors). The CHZ is defined here as the zone around a star where the planet's insolation flux lies between $0.2 S_{\oplus}$ and $2 S_{\oplus}$. Spinelli et al. 2023 select exoplanets by constraining their mass and radius to lie in between $0.1 M_{\oplus} \leq M_p \sin(i) \leq 10 M_{\oplus}$ and $0.5 R_{\oplus} \leq R_p \leq 2.5 R_{\oplus}$. It is clear from Figure 2 that in this research the M-dwarfs don't seem able to start abiogenesis, due to their low UV luminosity. CHZ planets around these stars are not located in the UHZ of their star. From this research and a scan of Hubble Space Telescope and SWIFT catalogues we found a gap in the UV flux data of stars with planets in the habitable zone. This thereby leads to a gap in our knowledge in terms of quantifying the potential habitability and holds the potential to revolutionise search for habitable planets. By combining and refining the UHZ and the CHZ, we can constrain the number of exoplanets that could potentially be habitable. Our definition of the CHZ is based on the distance from a star at which a planet receives optimal bolometric insolation flux (S), where conditions are neither too hot nor too cold for life (insolation flux between $0.2 S_{\oplus}$ and $2 S_{\oplus}$). By not constraining the planet's mass and radius, we try to understand whether complex molecules can also originate on non-rocky planets in for example their clouds.

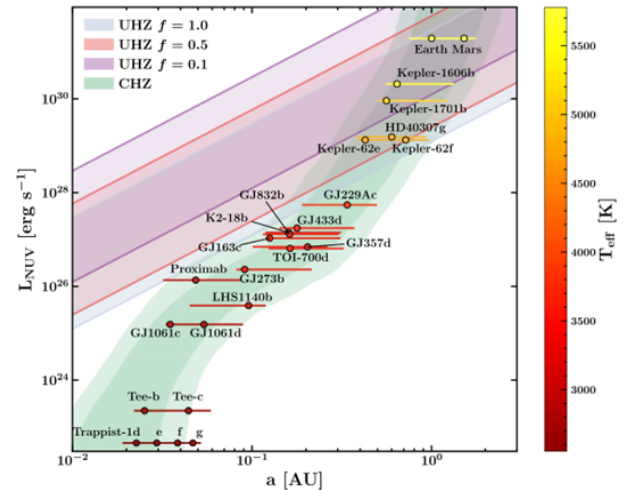


Figure 2: Planets in the optimistic circumstellar habitable zone (green) planets and UV habitable zone for 1.0, 0.5 and 0.1 transmission factor (Spinelli et al. 2023). Colour code shows stellar effective temperature.

1.3 Solar flares and light echoes: an important aspect of habitability

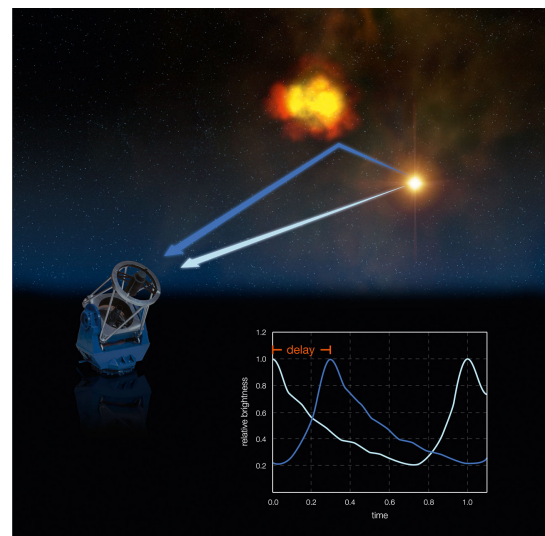


Figure 3: Light Echoes (Artist's impression) (ESO, 2018).

The concept of using light echoes of stellar flaring events to detect exoplanets relies on temporally resolving two outbursts of light: once from the host star, and a second emission by the light scattering of the planet (Sparks et al. 2018). Light echoes of stellar flares provide a challenging, but very useful detection method for close-in exoplanets as they are largely independent of system orientation. Analysing multiple flare events from the same star could provide valuable information on a planet's orbit, and physical properties (like albedo), providing a new method for extracting these parameters.

¹ Extremophiles are microorganisms that thrive in extreme environments

Echoes are light reflected by the planet itself, meaning that their strength depends on planet radius, albedo and orbital phase. They can arise from any viewing angle, but their strengths fall off quickly with distance. Thus the method is most sensitive to giant planets within 0.1 AU of actively flaring stars, due to high contrast ($> 10^{-7}$). (C. Mann et al., 2018) M-dwarfs, the most common spectral type stars, are particularly susceptible to this intense and frequent flaring events, being ideal candidates for this detection method. Their outbursts can occur up to 3 times per day in the line-of-sight. EXPOSURE will have an expected yield of about 20 habitable zone planets within 100 pcs.

Stellar flares have an important role in defining the above-mentioned UHZ as well. In order for life to form, a sufficient amount of UV is necessary for prebiotic photochemistry to happen and flares could be an important asset in that regard.

There are dozens of exoplanets that are in the liquid water habitable zone, but the question arises: could life start on these planets in the first place? Experiments have shown that the critical wavelength for the origin of life is between 200 and 280 nm in the UV spectrum (Rimmer et al. 2018). Ultracool stars produce a small amount of light in this range, therefore flares in fact, may be the only pathway to starting life on their planets. The equation gives us our constraint on which power laws are necessary for building up the prebiotic inventory is the following:

$$\nu = \frac{8 \times 10^{27} \text{ erg/s}}{E_U}$$

Evaluating the flare rates by this equation shows us the stars potentially hosting planets within their abiogenesis zones (% active). The highest flare rates are for stars between 0.6 to 0.7 M_{\odot} (table 3, Paul B. Rimmer et al. 2018).

2 Mission goal

Our mission will characterise exoplanets by studying the NUV emission from stars and the Lyman alpha absorption from exoplanet atmospheres. The mission will constrain and extend the concept of habitability to UV light received by the exoplanets from their host stars. Last but not least our mission will detect light echoes.

2.1 Mission Objectives

Our main Mission Objectives are the following:

Constrain evolutionary models of exoplanets by studying the occurrence and extent of their extended/evaporating hydrogen atmospheres as well as their variability

- **MO1** Detect hydrogen atmospheres of exoplanets in the liquid water constrained habitable zone with a radius equal or larger than 1.5 Earth radii
- **MO2** Detect escaping hydrogen atmospheres of exoplanets for planets >1.5 Earth radii and periods shorter than 30 days.
- **MO3** Conduct stellar monitoring observations to determine the variability in UV-flux from stars
- **MO3** Assist in monitoring stellar activity in the UV to improve atmospheric characterization conducted by other observatories (Ground-based or in space)
- **MO4** Determine a newly constrained habitable zone around a star in which an optimal amount of UV-radiation (200-280 nm) reaches the planet
- **MO5** Detect light echoes from exoplanets orbiting M-dwarfs to reconstruct their orbits and determine their albedos.

2.2 Scientific objectives and observational requirements

Our mission therefore has four main Observational Requirements:

- **S01** The mission shall do spectroscopy around the Lyman alpha line on stars with transiting planets in the habitable zone
- **S02** The mission shall do spectroscopy around the Lyman alpha line on stars with transiting planets which are predicted to have evaporating atmospheres
- **S03** Measuring variations in the UV emission of stars with planets in the habitable zone
- **S04** Temporarily resolve flare emission from star and re-emission by the exoplanet.

2.3 Driving Measurement requirements

For Spectroscopy

- **T-01** The spectral bandwidth shall be 2.5 ± 0.01 nm for S-02
- **T-02** The observed spectrum shall be centred around $121.56 \text{ nm} \pm 0.01 \text{ nm}$ for S-02
- **T-03** The spectral bandwidth shall be 15 ± 0.01 nm for S-01
- **T-04** The observed spectrum shall be centred around $122.5 \text{ nm} \pm 0.1 \text{ nm}$ for S-01
- **T-05** The spectral resolution shall be $20000'' \pm 100''$ for S-02
- **T-09** The spectral resolution shall be $1000'' \pm 100''$ for S-01

For Photometry

- **T-10** The poisson noise ratio shall be larger than 1000
- **T-11** The observation cadence shall be 30 seconds
- **T-12** The spectral bandwidth for case 2 shall be from $200 \pm 1 \text{ nm}$ to $280 \pm 1 \text{ nm}$

- **T-13** The spectral bandwidth for case 3 shall be from 100 ± 1 nm to 400 ± 1 nm

3 Targets

The targets in this mission are all selected from the NASA archive database (Akeson et al. 2013) and the Exoplanet.eu catalogue (Schneider et al. 2011). For all cases we use a distance of less than 100 pc in order to avoid UV light absorption from the interstellar medium. And a field of view between -70 and 70 degrees in ecliptic latitude due to the satellite requirements. We use the following constraints for the different science objectives:

For the extended atmospheres:

- G, K, M type stars
- Radius of the planet $< 2.5 R_{\oplus}$ ⁽²⁾
- distance from Earth of < 100 pcs
- $0.2S_{\oplus} < \text{insolation flux} < 2S_{\oplus}$ ⁽²⁾

For the escaping atmospheres:

- F, G, K, M type stars
- Radius of the planet $> 1.5 R_{\oplus}$ (exoplanets from super-Earths to larger)
- distance from Earth of < 100 pcs
- orbital period < 30 days (for higher orbital periods the atmosphere does not get inflated enough for it to escape)

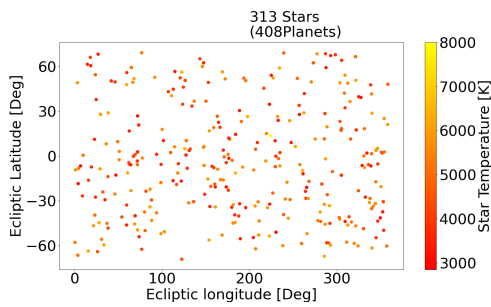


Figure 4: Example with targets between -70 and 70 degrees from the ecliptic plane. The plots for the other cases are not shown.

For the habitable zone:

- F, G, K, M type stars
- distance from Earth of < 100 pcs
- $0.2S_{\oplus} < \text{insolation flux} < 2S_{\oplus}$ (where planet receives optimal bolometric insolation flux)

² to observe rocky, Earth-like exoplanets in the CHZ with hydrogen atmosphere larger than $10 R_{\oplus}$.

For the light echoes:

- M-dwarf stars
- distance from Earth of < 100 pcs
- Orbital separation > 0.06 AU (if planet and star are too close the amount after flare from the star is too short to be observed)
- Contrast between star and planet of 10^{-7} (proportional to distance and size of the planet, most conservative scenario (Sparks et al. 2018))

	Escaping atmospheres	Extended atmospheres	Habitable zone	Light echoes
Stars	313	32	192	16
Planets	408	44	224	19

Table 1: Table showing the the number of targets for the different scientific objectives

4 Payload

4.1 Telescope

The telescope will be an off-axis Anastigmat telescope with a 4.2 m primary mirror and a f-ratio of $f/100$ which leads to a total focal length of 420 m. The focal length is reached by folding the light path using 2 mirrors. The telescope also contains a fine steering mirror relying on a fine-guidance sensor to provide precise pointing. The telescope is put off-axis to have maximum throughput.

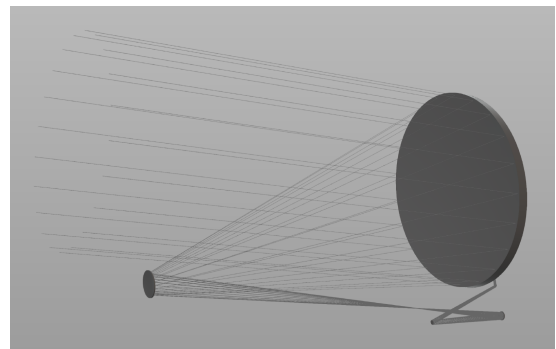


Figure 5: The Anastigmat Telescope of EXPOSURE

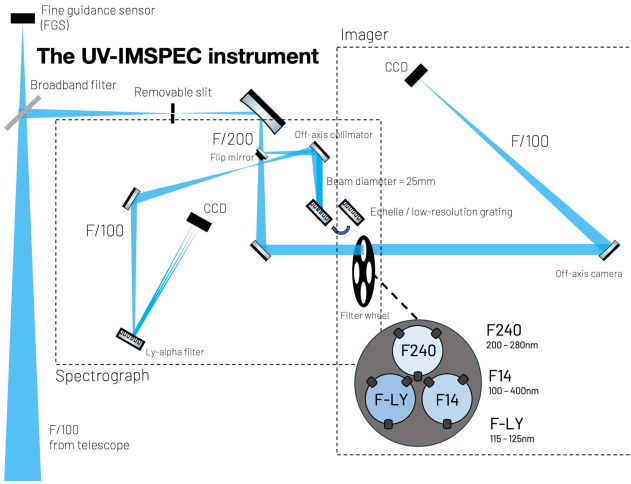


Figure 6: The Optical configuration of UV-IMSPEC

Due to the temperature of the host stars, UV thermal emission is only a fraction of the stellar luminosity. To be able to detect Light Echoes signals of Planets orbiting as close as 0.06 AU the temporal resolution must be smaller than 30 seconds. To resolve the contrast of $10e-7$ between the fluxes of the planet and the star with a 2σ significance a signal to noise ratio of 2000 needs to be achieved. Therefore, the minimum amount photons collected C_{min} can be derived.

From the stellar temperature and distance between the observing spacecraft and an assumption on the flux emitted by the star in the observed bandwidth F_{UV} the collecting area needed A_{min} can be calculated with following equation:

$$A_{min} = C_{min} \frac{E}{F_{UV}}$$

To be able to observe a significant amount (~30%) of the total population in the observed region, the telescope requires a 4.2 m telescope, assuming a throughput of 5 % (losses from the aperture until the detector). To be able to gain this throughput further development is needed.

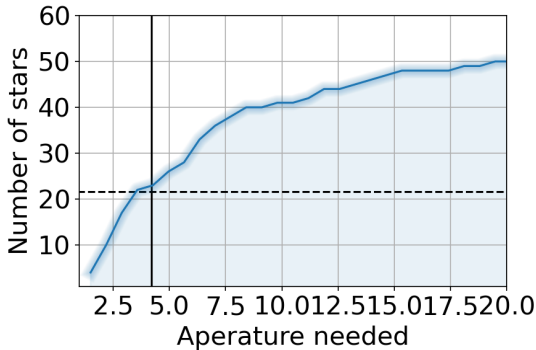


Figure 7: Number of stars observable depending on the aperture size assuming an 5 % throughput. Vertical line represents chosen aperture, vertical dashed line shows ~30% of the total population.

4.2 UV-IMSPEC

The Instrument on EXPOSURE called UV-IMSPEC will include an Imager and a Slit Spectrograph. In Figure 6 the optical path and parts are indicated.

The imager will be accompanied by 3 different filters (F240: 200-280 nm, F14: 100-400 nm, F-LY: 115 - 125). The components are optimised for high efficiency. Besides, we tried to minimise the amount of optical surfaces as any surface will absorb relatively much in the UV compared to the optical. Given the large aperture size, we were required to work with relatively slow beams to achieve Nyquist sampling. The spectrograph will be equipped with 2 different gratings with resolutions $R = 1000$ and 20000 .

Given the short wavelengths in the UV, our tolerances on RMS WFE are tight and we aim to keep them below 10 nm for the full optical train. To avoid scattering and related straylight the roughness of the optical surface shall be around 0.1 nm.

Detectors description

The instrument on EXPOSURE will feature a new UV detector technology, the Electron Multiplying Charge-Coupled Device (EMCCD). The EMCCD functions similarly to a nominal CCD, but has a second serial register containing additional pixels and an added high voltage clock. Electrons passing through the serial register are multiplied through impact ionisation, which has the major advantage of increasing the signal from a single photoelectron to a value much larger than the on-chip amplifier read-out noise. The EMCCD also amplifies clock-induced-charge (CIC) and dark current. CIC is minimised by operating in non-inverted mode (NIMO), while evidence suggests that dark current noise plateaus below an operating temperature of -110°C . These properties make the EMCCD an attractive detector for use in the UV spectral range, where the efficiency and throughput of optical design is lacking. The EMCCD has been demonstrated successfully during multiple flights on the NASA/CNES balloon-borne UV multi-object spectrograph, the Faint Intergalactic Red Shifted Emission Balloon (FB-2).

5 Key Drivers

Several key system drivers were determined for the service module, which have to be thoroughly respected. For instance, it shall be necessary to consider a data amount of 240GB/day, a distance between main and secondary mirrors of 7 metres and a pointing accuracy of 0.1 arcsec for the spacecraft.

It is required for the orbit position to remain outside of the Earth's geocorona (to prevent Lyman-alpha absorption), and for the nominal mission duration to be of 6.5 years, plus an extension of 3.5 years. Finally, the ground station access shall be ensured by ESTRACK'S Deep Space Network.

6 Mission Analysis

For this mission, a halo orbit around the Sun-Earth L2 Lagrange point, with an apoapsis altitude of 8.52×10^5 km and periapsis altitude of 2.5×10^5 was chosen. This option allows for the telescope to remain outside Earth's geocorona, which is known for absorbing Lyman-alpha, and thus for disturbing observations in this specific wavelength.

The telescope shall be launched in 2038 from an Ariane 6.2, in a launch window that allows us to avoid Earth and Moon eclipses during transfer. After the separation from the launcher, the spacecraft shall start with the early operations mode, where the sun shield and the secondary mirror structure unfolds. After this, an initial manoeuvre is required due to the launcher's dispersion (<50 m/s).

Secondly, the telescope shall be inserted in a stable manifold transfer allowing it to reach the target orbit, during which further service module commissioning actions can be done, which are only halted during an additional mid course correction (5 m/s).

Upon reaching L2, the payload commissioning starts. Consequently, nominal operation begins the targeting and observation of a field of interest. This is repeated several times, only halted by desaturation events of the reaction wheels (1 m/s / year) and orbit maintenance manoeuvres (1 m/s / year). At the end of the mission, the telescope shall be decommissioned into a graveyard heliocentric orbit (20 m/s). An overall delta-V of 115 m/s is required for nominal and extended mission lifetime.

7 Spacecraft design

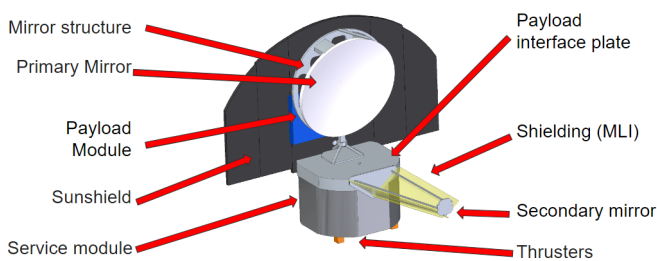


Figure 8: Spacecraft design

The design of the spacecraft is presented in Figure 8. At the bottom, the service module with its 12 thrusters is visible. It contains the Attitude & Orbit Control, Communication, Electric Power System and Thermal subsystems. A foldable sunshield attached at the back protects the mirrors from the stray light effect. The payload is attached to the spacecraft with the help of an interface plate. Both the main mirror, with a diameter of 4.2 metres and secondary mirror with a diameter of

0.5 metres are mounted on a tripod to remain isostatic. Thrusters for the propulsion subsystem are attached at the bottom of the spacecraft.

During launch, the arm with the second mirror is folded to fit into the payload fairing of the Ariane 6.2 rocket. It is held vertically by a hold down release mechanism (HDRM) above the main mirror.

8 Propulsion

The propulsion system is used for orbital manoeuvres (injection, maintenance, and disposal) and desaturating the reaction wheels. Therefore, 12 thrusters are positioned on the bottom side of the service module in groups of 3 which are located 90° apart. This allows the unloading of all 3 axes. In such a configuration, 4 thrusters are located in Y- (see Fig. 8) which can be used together to quadruple the thrust level for orbital manoeuvres. Due to the configuration, the propulsion system can compensate for a loss of thrusters.

As a trade-off between complexity and efficiency a blow-down system with 5N monopropellant hydrazine thrusters is used with a specific impulse of 220 s. For nominal and extended lifetime 187 kg of propellant and 3 kg of pressurizer gas (Helium) are required.

9 Attitude Control System & Orbit Control System

To achieve the necessary level of aiming accuracy (0.1 arcsec) for scientific purposes and 3-axis stabilisation, the spacecraft requires a very accurate attitude determination and control system. For this reason, numerous sensors are used.

The Attitude Determination System is equipped with 6 sun sensors (2 redundant) which provide the accuracy of ~ 1 arcmin (Fortescue et al. 2011). The final precision is improved to the ~ 1 arcsec by the use of 4 star trackers (1 redundant). Due to the need to keep the spacecraft in the correct orientation even in the event of a failure, a redundancy must be used, adding several spare sensors of each type. The FGS sensors (included in the payload, 1 redundant) serve also as part of the ACS and is crucial for achieving appropriate pointing accuracy at ~ 0.1 arcsec. 2 accelerometers (1 redundant) and 2 gyroscopes (1 redundant) are used to determine relative attitude and rotational movement.

Four reaction wheels (1 redundant) are used as active actuators. Their desaturation takes place through the use of thrusters from the propulsion subsystem.

10 EPS

The electric power system consists of solar arrays and a power conditioning distribution unit including batteries from DHV Technologies. Analysing the power consumption of each subsystem in each mode gives a total power requirement per mode. The following figure shows the power distribution to each subsystem during imaging with the number inside the pie chart being the power requirement in Watts. While the most time is spent imaging, the power consumption is highest during desaturation events (349 W).

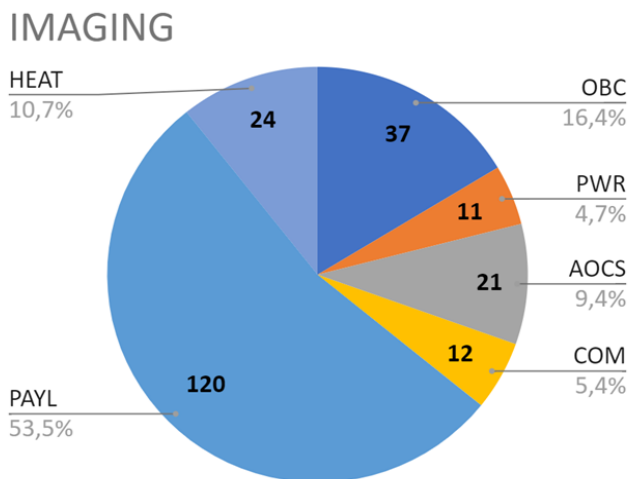


Figure 9: Power requirement of each subsystem during imaging

Therefore, the solar panels are sized for this situation. 6m² solar panels are used, producing 1950 W. However, the telescope's pointing requirements means that the solar panels are not pointed directly towards the sun. This, but also the solar panel's degradation has to be taken into account. This reduces the end of life power generation including the pointing error to 545 W.

The solar panels power output is conditioned and distributed by a power module including 6x 1600 Wh LiFePO₄ battery packs. As there are no eclipses, there should not be time with no power generation. However, in emergency situations the spacecraft shall bridge 8h to return to nominal operation.

11 Ground Segment & Communications

Given the long distance from Earth to L2, it is necessary to use the ESTRACK Deep Space 35m antennas, namely the Cebreros (Spain), Malargüe (Argentina) and New Norcia (Australia) ground stations. Each is commanded from the European Space Operations Center (ESOC) in Darmstadt, Germany.

While the first two antennas will be used for both the telescope's housekeeping and science data transmission, in the Ka-band, New Norcia shall only be resorted to during safe mode, using S-band. For housekeeping telemetry and transmission, a frequency of 32GHz downlink and 34.6 GHz uplink will be used, whereas for Science Data Transmission the corresponding values shall be of 31.8GHz downlink and of 34.3GHz uplink.

The spacecraft shall be equipped with two 0.26m diameter Ka-band high-gain gimballed antennas, and two 0.2m S-band medium-gain antennas, with downlink and uplink frequencies of 2200MHz and 2050MHz, respectively. As a result, the telecommunications subsystem is redundant.

Finally, a data rate of 130Mbps shall be used, which translates into a data amount of 240 Gigabytes per day, considering a time interval of 4 hours and 6 minutes between acquisition and loss of signal.

12 On-Board Computer

In order to minimise the risk in the mission, it was decided to use components previously used in a similar environment, with the use of redundancy. The 2 on-board (primary and redundant) radiation hardened computers with RAD750 processor, having a TRL 9 and previously used in the JWST mission, were selected.

The scientific data produced in one day is 240GB. Despite the fact that it can be sent to Earth within about 4 hours daily, it was decided to use 1 TB of storage, so that in the event of a failure of the communication system, all the data collected by the payload instruments will be able to be collected up to 4 days later.

13 Thermal Control

The detector temperature is the primary driver in designing the thermal subsystem, which must be kept within [153 K; 233 K]. Passive thermal control is mainly achieved using a thermal/sun shield and classical highly-insulating multi-layer blankets. A 1.23m² radiator has been positioned in the area of the spacecraft that is always shielded from the sun, on the back of the solar shield attached to the payload. It is used to dissipate the excess power (worst-case scenario 500 W), designed based on the radiative thermal exchange between the spacecraft, the incoming solar flux, and the Earth's IR radiation flux along the orbit. The white paint's optical properties are chosen for the radiators. Thermostats with heaters control batteries, gyroscopes, reaction wheels, and hydrazine tanks at optimal operating temperatures.

14 Budgets

Subsystem	Mass [kg]
ACS	380
COM	36
EPS	79
PAYLOAD & INSTRUMENTS	350
STR	1419
THE	10
OBC	25
OCS	314
SUMMARY	2613

Table 2: Mass budget

	Category	Cost [M€]
Service Module	Industrial Cost	450
Telescope & Instruments	Industrial Cost	450
-	ESA project cost	170
	Operations	80
	Total	1150
	Total (20% margin)	1380
	Launch	100
Delivery to L2	Payload provided by ESA member states	-10 (10% of LAUNCH)
	Summary	1420

Table 3: Cost budget

15 Risk assessment

The Electron Multiplying Charge-Coupled Device (EMCCD) is TRL5, and this risk should be mitigated by including it on a smaller pathfinder mission prior to the launch of EXPOSURE in order to flight qualify the part. A risk of Single Event Upsets (SEU's) was identified in the OBC and should be mitigated by having redundancy and FDIR capability. In case of degradation of the primary mirror or coatings of other optical components, the noise level will increase, and this can be mitigated by using a longer exposure.

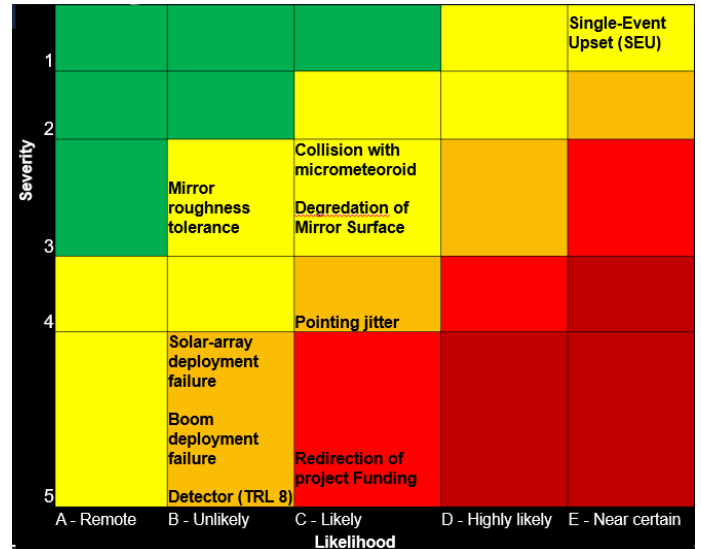


Figure 10: Risk matrix with mitigation

16 Descope options

In case the mission turns out to be unfeasible due to financial restrictions, two descope options may be considered, at the cost of certain observational requirements. Firstly, it's possible to reduce the diameter of the telescope at the expense of less sensitivity, leading to the exclusion of requirements O-4: Light Echoes or O-1:Hydrogen Atmospheres.

Alternatively, would consist in the removal of the imager instrument, which would exclude requirements O-4: Light Echoes as well, or O-3:UV variability.

17 Public Outreach and Extended Mission Phase

Public outreach is a fundamental aspect of science as engaging the public in space exploration is highly beneficial for promoting space missions and satellite mission fundings. Before and after launch we plan to provide the public with educational materials and news articles on exoplanetary science, including habitability and life on other planets. We will give updates on the EXPOSURE development on our social media. We allow for the possibility to extend our mission, if needed. Also, we propose to start outreach well before launch, to increase engagement, and inspire next generations of physicists, astronomers, and engineers.

18 Conclusions

EXPOSURE is an ambitious mission which characterises exoplanets in the UV range. This mission will fill the gap in the UV range, presenting unprecedented advances for a better understanding of formation and evolution of exoplanets,

including redefining our ideas of habitability. Moreover, EXPOSURE will complement other exoplanet missions such as PLATO, ARIEL, CHEOPS, and JWST. Last but not least, EXPOSURE will be the first large scaled survey for light echoes detection from exoplanets.

19 References

- Attia, O., et al. "The Jade Code: Coupling Secular Exoplanetary Dynamics and Photo-Evaporation." *arXiv.Org*, 3 Mar. 2021
- Batygin et al. "Formation of Rocky Super-Earths from a Narrow Ring of Planetesimals." *arXiv.Org*, 11 Jan. 2023
- Brož, M., et al. "Early Terrestrial Planet Formation by Torque-Driven Convergent Migration of Planetary Embryos." *Nature News*, 5 July 2021
- Lecavelier Des Etangs, A., et al. "Evaporation of the Planet HD 189733b Observed in H I Lyman- α ." *NASA/ADS*,
- Charnoz, Sébastien, et al. "The Effect of a Small Amount of Hydrogen in the Atmosphere of Ultra Hot Magma-Ocean Planets: Atmospheric Composition and Escape." *Astronomy & Astrophysics*, 26 June 2023
- do Amaral. *The Contribution of M-Dwarf Flares to the Thermal Escape ... - Iopscience*., Accessed 19 July 2023.
- JM;, Atri D;Hariharan B;Grießmeier. "Galactic Cosmic Ray-Induced Radiation Dose on Terrestrial Exoplanets." *Astrobiology*
- Johnstone et al. "*The Active Lives of Stars: A Complete Description of the Rotation AndLess Effective Hydrodynamic Escape of H₂-H₂O Atmospheres ...*" *Iopscience*
- Mandell, Avi M., et al. "Formation of Earth-like Planets during and after Giant Planet Migration." *NASA/ADS*
- Mol Lous, Marit, et al. "Potential Long-Term Habitable Conditions on Planets with Primordial H-He Atmospheres." *Nature News*, 27 June 2022,
- Mordasini, C., et al. "Characterization of Exoplanets from Their Formation. I. Models of Combined Planet Formation and Evolution." *NASA/ADS*,
- Owen, James E., and Dong Lai. "Photoevaporation and High-Eccentricity Migration Created the Sub-Jovian Desert." *arXiv.Org*, 29 June 2018,.
- Owen, James E. et al. "Kepler Planets: A Tale of Evaporation." *NASA/ADS*,
- Pierrehumbert et al., "*Climate of the Neoproterozoic (N.d.)*"
- Vidal-Madjar, A., et al. "An Extended Upper Atmosphere around the Extrasolar Planet Hd209458b." *NASA/ADS*,
- Yoshida et al. "*Less Effective Hydrodynamic Escape of H₂-H₂O Atmospheres*"
- Zeng, Li, et al. "Growth Model Interpretation of Planet Size Distribution." *Proceedings of the National Academy of Sciences*, vol. 116, no. 20, 2019, pp. 9723-9728
- Sagan, Carl.. "Ultraviolet selection pressure on the earliest organisms." *Journal of theoretical biology* 39 1 (1973): 195-200 .
- Cockell, C. S. (1998), Biological effects of high ultraviolet radiation on early earth—a theoretical evaluation, *Journal of Theoretical Biology*, 193(4), 717-729, doi:https://doi.org/10.1006/jtbi.1998.0738. 1
- Kopparapu et al. (2013) HABITABLE ZONES AROUND MAIN-SEQUENCE STARS: NEW ESTIMATES, *The Astrophysical Journal* ,765 (2), 131, doi:10.1088/0004-637x/765/2/131. 1, 2
- Kopparapu et al.(2014), Habitable zones around main-sequence stars: dependence on planetary mass, *The Astrophysical Journal Letters* ,787(2), L29. 2
- Spinelli, R., F. Borsa, G. Ghirlanda, G. Ghisellini, and F. Haardt (2023), The ultraviolet habitable zone of exoplanets, *Monthly Notices of the Royal Astronomical Society*,522 (1), 1411-1418, doi:10.1093/mnras/stad928. 1
- Akeson, R. L., et al. "The NASA exoplanet archive: data and tools for exoplanet research." *Publications of the Astronomical Society of the Pacific* 125.930 (2013): 989.
- J. Schneider et al., Defining and cataloguing exoplanets: the exoplanet.eu database. *A&A* 532 A79 (2011)
DOI: 10.1051/0004-6361/201116713
- Buccino et al., "UV Habitable Zones around M Stars." *Icarus* 192.2 (2007): 582-587.
- Kyne, et al. "Delta-doped electron-multiplying CCDs for FIREBall-2." *Journal of astronomical telescopes, instruments, and systems* 6.1 (2020): 011007-011007.
- P. Fortescue et al. (2011), "Spacecraft Systems Engineering"
- D. R. Akins et al. (2004), "ESA/ESOC 35-Meter Deep Space Antenna Front-End Systems"
- Ritson et al. "Prebiotic synthesis of simple sugars by photoredox systems chemistry." *Nature chemistry* 4.11 (2012): 895-899.
- Rimmer et al. (2018), The origin of rna precursors on exoplanets, *Science Advances*, 4
- C.Mann et al. 2018, *The Astronomical Journal*, doi: 10.3847/1538-3881/aadc5e
- Gul, F. et al. (1986), Foundations of dynamic monopoly and the coase conjecture, *Journal of Economic Theory*, 39 (1), 155-190
- Sparks, William B., et al. "The direct detection and characterization of M-dwarf planets using light echoes." *The Astrophysical Journal* 854.2 (2018): 134.
- Brož, M., et al. "Early terrestrial planet formation by torque-driven convergent migration of planetary embryos." *Nature Astronomy* 5.9 (2021): 898-902.
- Young, A. V., et al. "Constraining Chemical Disequilibrium Biosignatures for Simulated Remote Observations of an Earth-like Exoplanet." *NASA/ADS*, ui.adsabs.harvard.edu/abs/2021AAS...23723005Y/abstract. Accessed 19 July 2023.